



Numerical Analysis of an Unsaturated Capillary Barrier Cover System

Mohammad Ali Hagh Shenas^{a#} and Hassan Sharafi^{a†}

^a *Department of Civil Engineering, Faculty of Engineering, Razi University, Iran.*

Authors' contributions

This work was carried out in collaboration among all authors. All authors contributed to the study conception and design. Material preparation, data collection and analysis were performed by authors MAHS and HS. The first draft of the manuscript was written by authors MAHS. All authors commented on previous versions of the manuscript.

Article Information

DOI: 10.9734/JERR/2021/v21i1017498

Open Peer Review History:

This journal follows the Advanced Open Peer Review policy. Identity of the Reviewers, Editor(s) and additional Reviewers, peer review comments, different versions of the manuscript, comments of the editors, etc are available here: <https://www.sdiarticle5.com/review-history/81417>

Short Research Article

Received 22 October 2021
Accepted 25 December 2021
Published 26 December 2021

ABSTRACT

Inclined multi-layered barriers can be used to protect underlying waste storage facilities. The intended barriers can be used to confine the infiltration through implementation of the capillary barrier effect. In this study, the effect of rainfall, evaporation, and transpiration on the hydraulic properties of inclined covers was assessed by performing a series of simulations using HYDRUS-2D numerical models. The material of the intended layers included clay loam soil as a seepage control layer, sandy soil as a moisture retention layer, and gravel as a capillary break layer. Based on the key results of numerical analyses, Lateral diversion in the interface between the seepage control layer and moisture retention layer occurred as a result of the significant slope of said layers and the low permeability of the moisture retention layer. At the reduced degree of saturation, water did not move easily from the seepage control layer to the moisture retention layer as well as from the moisture retention layer to the capillary break layer due to the low hydraulic conductivity. The negative pressure head in the seepage control layer had minimal effect on the water content in the moisture retention layer. Hence, the performance of this protective earthen cover can, then, be guaranteed due to the current climatological conditions.

Keywords: *Capillary cover barriers; retention capacity; hydraulic properties; suction; volumetric water content.*

[#] *Ph.D. Candidate,*

[†] *Assistant Professor,*

^{*}*Corresponding author: Email: H_SHARAFI@RAZI.AC.IR;*

1. INTRODUCTION

In humid regions, waste can be considered a serious threat to ground water due to percolation from infrastructures such as landfills, which are the current preferred solution for disposal [1].

A multi-layer capillary barrier cover system is designed to reduce percolation in humid, arid, and semi-arid climates [2-6].

The percolation into underlying waste in these regions can be reduced through covers made up of earthen materials for promotion of the capillary barrier effect [7-11]. Earthen covers are designed in various forms but are comprised of multi-layered contrasting particle sizes that consist of fine-grained and coarse-grained sediments [12-17,9]. The water movement restriction across the interface of these layers occurs due to the contrast in unsaturated hydraulic properties employed by the materials [18,19].

The anisotropic ratio (K_x / K_y) is described as soil hydraulic conductivity anisotropy, where K_x and K_y are the hydraulic conductivity in the horizontal and vertical directions, respectively. The values of the anisotropic ratio for clay soil can be higher than 100 [20]. Laboratory and field experiments have been shown that the amount of hydraulic conductivity anisotropy is related to the degree of water saturation [21]. The degree of anisotropy has been explained by the anisotropy factor, defined as the ratio of diagonal components of the hydraulic conductivity tensor [22].

The results in transient seepage analysis and slope stability analysis show that when the vertical hydraulic conductivity (K_y) is constant, the horizontal hydraulic conductivity (K_x) increases (*i.e., anisotropy increases*) [23]. Increased hydraulic conductivity anisotropy ratio will cause a slower infiltration rate in the vertical direction at the toe of the slope [23].

The present study intends to investigate the water balance of a multi-layer earthen cover. The purposes of current research are to minimize leachate transport by infiltrating water and reduce erosion of earthen covers by water and wind. The unsaturated hydraulic performance of the earthen barrier is numerically evaluated under different climatological conditions spanning the past 20 years (2000-2019) in Canada (Windsor)(Fig.1).

For this purpose, the useful finite element code HYDRUS-2D was used to investigate the water flux that leaves the barrier. The generated water flux was investigated as vertical infiltration and as lateral flux. The numerical simulation was done for a multi-layer earthen barrier. Design parameters, such as layer thickness and geoenvironmental parameters of materials, follow the "Landfill Gas Collection and Control Regulation" of Ontario.

The program used for this study – HYDRUS – is a modeling environment for the analysis of water flow and solute transport in variably saturated porous media. HYDRUS uses computational finite element models for the two- and three-dimensional simulation of solutes and water through said media. The model is supported by an interactive graphics-based interface for data-preprocessing, generation of structured and unstructured finite element mesh, and graphic presentation of the results [24].

2. MATERIALS AND METHODS

2.1 Location and Area

Essex County locates in the southwestern end of Southern Ontario. The only land boundary on the east is Kent County. It is bounded by the Detroit River to the west, Lake St. Clair to the north, and Lake Erie to the south. The city of Windsor in the northwest section of the County is 188.7 km from London and 365.8 km from Toronto.

2.2 The Classification and Description of Essex County Soils

Soil horizons are grouped under three main parts. The first layer has been filtrated of some mineral constituents but contains an accumulation of organic materials in the upper part. The second layer is usually darker in color and heavier in texture than the first layer and the structural aggregates are well formed. The parent material from which the soil has developed is defined as the third layer.

2.3 Climate

Essex County is the earliest and warmest part of the Ontario province. The lowest annual precipitation, only 28.1 inches; its average snowfall is only 32 inches. In the rest of the county the mean annual temperature is 8.3°C.

2.4 Barrier Design

Earthen barriers are usually made up of fine-grained sediment overlying coarse-textured soil. The simulated multi-layer capillary barrier consists of natural materials. The selected materials for this study's modelled barrier are clay loam as the seepage control layer, sand as the moisture retention layer, and gravel as the capillary break layer. Additionally, the layer has a slope of 10%, which, based on "Landfill Gas Collection and Control Regulation" of Ontario, the slope can be between 5% and 25%. The slope performance includes water percolation discharge and lateral diversion. The purpose of the top 0.6 m of clay loam is to serve as the seepage control layer to reduce water percolation, bio-intrusion, and water storage, as well as promote plant growth. The underlying layers include 0.4 m of sand and 0.2 m of gravel that are used as capillary break, to prevent downward infiltration of water as well as excess-water discharge. A cross-section of the designed cover is depicted in Fig.2.

An essential part of protective earthen cover is vegetation. In this study, evapotranspiration was indirectly accounted for by using the Hargreaves equation [25,26]. Likewise, soil evaporation and plant transpiration were calculated using Beer's law, which divides the solar radiation component of the energy budget via interception by the canopy [27,28].

The numerical analysis of water flow was confined to the three-layered barrier. The numerical simulation was done by a fine computational mesh, as demonstrated in the different layers. This is an essential part in the transient state of water flow modelling. Also, it is to be noted that the hydraulic properties of unsaturated materials have a non-linear behavior.

Knowledge about the hydraulic properties of the chosen barrier materials – clay loam, sand, and gravel – help to understand the hydraulic behavior of the layers. The intended hydraulic properties are soil water retention curve, $\theta(h)$; and hydraulic conductivity function, $K(h)$; where h is pressure head, θ is volumetric water content, and K is hydraulic conductivity. The hydraulic properties of the materials were not obtained based on real measurements. The hydraulic properties of clay loam were obtained by RETC code [29] while the hydraulic properties of sand and gravel were selected from literature. A short

review of the selected hydraulic properties is presented below (parameter values will be discussed in Table 1).

2.5 Governing Flow Equation

Based on the two-dimensional isothermal uniform Darcian flow in a porous medium with variably saturated conditions, which the air phase does not consider in the water flow process, Richards' equation has been modified to introduce the governing flow equation. The modified Richard's equation, then, appears as:

$$\frac{\partial \theta}{\partial t} = \frac{\partial}{\partial x_i} \left[K \left(K_{ij}^A \frac{\partial h}{\partial x_j} + K_{iz}^A \right) \right] - S \quad (1)$$

where θ is the volumetric water content [$\frac{L^3}{L^{-3}}$], h is the pressure head [L], S is a sink term for plant water uptake [T^{-1}], x_i ($i=1,2$) are the spatial coordinates [L], t is time [T], K_{ij}^A is anisotropy tensor to account for the anisotropy medium K^A , and K is the unsaturated hydraulic conductivity function [LT^{-1}]. The unsaturated hydraulic conductivity function is presented by

$$K(h, x, z) = K_s(x, z)K_r(h, x, z) \quad (2)$$

where K_r is the relative hydraulic conductivity and K_s the saturated hydraulic conductivity [LT^{-1}]. Applying equation (3) to planar flow in a vertical cross-section would then introduce $x_1 = x$ as the horizontal coordinate and $x_2 = z$ as the vertical coordinate, the latter coordinate taken to be positive upward [24].

2.6 Unsaturated Soil Hydraulic Properties

The RETC Code is a computer program to analyze or predict the unsaturated hydraulic properties of soils: Water Retention Curve, $\theta(h)$; and Hydraulic Conductivity Function, $K(h)$. The hydraulic properties of soils are the key parameters used in water flow quantity analysis in unsaturated soils [29]. The soil-hydraulic functions used by van-Genuchten [30] included the statistical pore-size distribution model of Mualem [31] to obtain a predictive equation for the unsaturated hydraulic conductivity function in terms of soil water retention parameters. The expressions of van-Genuchten [30] are presented by equations (3), (4), and (5).

$$\theta_h = \begin{cases} \theta_r + \frac{\theta_s - \theta_r}{[1 + |\alpha h|^n]^m} & h < 0 \\ \theta_s & h \geq 0 \end{cases} \quad (3)$$

$$K(h) = K_s S_e^l [1 - (1 - S_e^{1/m})^m]^2 \quad (4)$$

Where $m=1-1/n$ (4)

The above equations contain six independent parameters:

θ_r (residual water content), θ_s (saturated water content), α, n (constant that define the curve shape),

K_s (saturated hydraulic conductivity), and l (pore-connectivity parameter). The pore-connectivity parameter in the hydraulic conductivity function was estimated [Mualem, 1976] to be about 0.5 as an average for many soils.

As depicted in Fig. 4, there are vast differences among the shape of soil hydraulic functions and the hydraulic behavior of soils.

The trail of soil types is as follows (Fig. 2): clay loam (upper material), sand (intermediate material) and gravel (bottom material). The barrier is characterized by a slope of 10%, a width of 10 m, and a depth of 1.2 m that includes the three mentioned layers of various thickness. The barrier consists of 4350 triangular elements present in areas where the highest fluxes occurred and where the more minute elements were considered.

2.7 Initial and Boundary Conditions

The solution of the modified - Richards' equation used in this research requires knowledge of the initial water content in the flow domain. The following equation serves that purpose.

$$\theta(x, z, t) = \theta_0(x, z) \text{ for } t = 0 \quad (6)$$

In (6), θ_0 is a determined function of x and z . There are three types of conditions that are described by HYDRUS to evaluate the system-independent interactions along the boundaries of the flow region. The pressure head (Dirichlet type) boundary conditions can be presented as follows:

$$h(x, z, t) = \psi(x, z, t) \text{ for } (x, Z) \in \Gamma_D \quad (7)$$

The described flux (Neumann type) boundary condition is presented by

$$-K \left[K_{ij}^A \frac{\partial h}{\partial x_j} + K_{iz}^A \right] n_i = \sigma_1(x, z, t) \text{ for } (x, Z) \in \Gamma_N \quad (8)$$

As well as the described gradient boundary conditions are presented by

$$\left[K_{ij}^A \frac{\partial h}{\partial x_j} + K_{iz}^A \right] n_i = \sigma_2(x, z, t) \text{ for } (x, Z) \in \Gamma_g \quad (9)$$

The Dirichlet, Neumann, and gradient type boundary segments are defined by $\Gamma_D, \Gamma_N, \Gamma_g$ respectively; $\psi [L], \sigma_1 [LT^{-1}],$ and $\sigma_2 [-]$ are prescribed functions of x, z and t , and n_i are the segments of the outward unit vector normal to boundary Γ_N or Γ_g [24]. In the HYDRUS program, the simulation of free drainage from a deep soil profile can be presented by the implementation of a gradient boundary condition in terms of a unit vertical hydraulic gradient. This circumstance is usually presented in the vadose zone studies (Sisson 1987; [21]).

In the present numerical simulation, the atmospheric boundary conditions are assigned to the top boundary and the free drainage boundary conditions are assigned to the bottom boundary (Fig.2). In the atmospheric boundary conditions, the external conditions control the potential fluid flux that moves across the intended boundary. Also, the actual flux depends on the dominant soil moisture conditions. The numerical solution of the modified form of Richards' equation is as follows:

$$\left| K \left[K_{ij}^A \frac{\partial h}{\partial x_j} + K_{iz}^A \right] n_i \right| \leq E \quad (10)$$

$$h_A \leq h \leq h_S \quad (11)$$

where E is the maximum potential rate of infiltration or evaporation under the current atmospheric conditions, h is the pressure head at the soil surface, and h_A and h_S are the minimum and maximum pressure heads allowed under the dominant soil conditions — respectively. Based on the HYDRUS assumption, any excess water on the soil surface is immediately eliminated [32]. Gradient type boundary conditions, exclusively as the unit gradient boundary condition or the Free Drainage boundary condition, were implemented by HYDRUS. Whenever the flow is contrary to the particular axis, the gradients in the x -direction (from right to left) and in the y -direction (from back to front) are positive [24].

The long-term daily climatological data – comprised of precipitation, evaporation, and transpiration — is assigned to the top boundary condition (the meteorological stations are "Windsor Riverside" and "Windsor A" which are situated in Windsor city, Ontario province, Canada), while a unit vertical gradient corresponds to simulate free drainage in the bottom boundary condition. The right and left boundaries of the domain assume zero flux boundary conditions. The initial water content for each soil type is included in Table 1 and it was considered throughout the barrier.

2.8 Numerical Solution Strategy

The initial water content at field capacity is calculated as follows:

$$S_{fc} = \frac{\theta_{fc} - \theta_r}{\theta_s - \theta_r} = n^{-0.6(2 + \log \theta_{10}^{K_s})} \quad (12)$$

where θ_{fc} and S_{fc} are the water content and saturation at field capacity, respectively. θ_r , θ_s , n , and K_s are the soil hydraulic parameters for the van Genuchten model [33]. The water content at field capacity corresponds to the hydraulic conductivity of about 0.01 cm/d.

The Galerkin finite element method with linear basis functions was used to obtain the solution for the modified form of Richards' equation dependent on the imposed initial water content and boundary conditions. Either the Gaussian elimination or the conjugate gradient method was used to solve each iteration system of linearized algebraic equations. The iterative process was continued until a satisfactory degree of convergence was obtained, i.e., until at all nodes in the unsaturated region, the absolute value of change in water content between two consecutive iterations became less than some small value determined by the imposed absolute value of water content ($0.0003 \frac{cm^3}{cm^3}$) tolerance.

2.9. Water Balance Computations

Water balance computations were performed 480 times for the three subregions of flow domain. The water balance information for each subregion is comprised of the actual volume of water, $V(cm^2)$, in the respective subregion; and the rate, $O (cm^2/day)$, of inflow or outflow to or from the subregion. V and O are given by

$$V = \sum_e \kappa \frac{\theta_i + \theta_j + \theta_k}{3} \quad \text{for 2D} \quad (13)$$

$$O = \frac{V_{new} - V_{old}}{\Delta t} \quad (14)$$

where $\theta_i, \theta_j, \theta_k$ are calculated water contents at the corner nodes of element e , and where V_{new} and V_{old} are volumes of water in the subregion computed at the current and previous time levels, respectively. The absolute error in the mass balance is computed by

$$\varepsilon_a^w = V_t - V_0 + S_t \int_0^t T_a dt - \int_0^t \sum_{n_r} Q_n dt \quad (15)$$

where V_t and V_0 are the volumes of water in the flow domain at time t and zero, respectively, as calculated with equation (12). The third term on the right side of the equation represents the cumulative root water uptake amount, while the fourth term gives the cumulative flux through nodes (n_r) located along the boundary of the flow domain or at internal source and sink nodes.

The accuracy of the numerical solution is evaluated in terms of the relative error, ε_r^w [%], in the water mass balance as follows:

$$\varepsilon_r^w = \frac{|\varepsilon_a^w|}{\max[\sum_e |V_0^e - V_t^e|, S_t \int_0^t T_a dt - \int_0^t \sum_{n_r} |Q_n| dt]} \quad (16)$$

where V_t^e and V_0^e are the volumes of water in element e at times t and zero, respectively. Note that HYDRUS does not relate the absolute error to the volume of water in the flow domain, but instead to the maximum value of two quantities. The first quantity represents the sum of the absolute changes in water content over all elements, whereas the second quantity is the sum of the absolute values of all fluxes in and out of the flow domain. This criterion is much stricter than the usual criterion involving the total volume of water in the flow domain; this is because cumulative boundary fluxes are often much smaller than the volume in the domain, especially at the beginning of the simulation.

Also, the water balance was calculated throughout the flow domain, made up of the three subregions previously adopted.

3. RESULTS AND DISCUSSION

Based on assigned initial water content and boundary conditions, flow in the multi-layer earthen cover was transient. The mean pressure

head in all layers is not constant (Fig.5). The water balance error at transient state, computed with equation (15), reveals the water balance error to be variable between 0.028% and 0.156%.

The total flux that leaves the simulation domain across the bottom boundary presents several noticeable features (Fig. 5). The main reasons that explain water drainage are water infiltration into the barrier, run-off from the sloping soil, and a rapid decrease in flux due to water drainage from the bottom. When the flux increased and was followed by a decrease, water drainage from either sand or gravel layers was considered.

The spatial variation of the Darcy flux across the bottom boundary is displayed in Fig. 6. The number of FE element associated with each node on the cross-section is the main factor during velocity calculation. A decreasing behavior was observed in an area close to the left and right boundary of the barrier. This is the result of number of FE connected with each node through the bottom boundary. The number of the nodes in the bottom boundary is 101.

Note that primary results of the Richards solution are the pressure heads. The pressure head and the velocity have direct relation.



Fig. 1. The map of Widsor

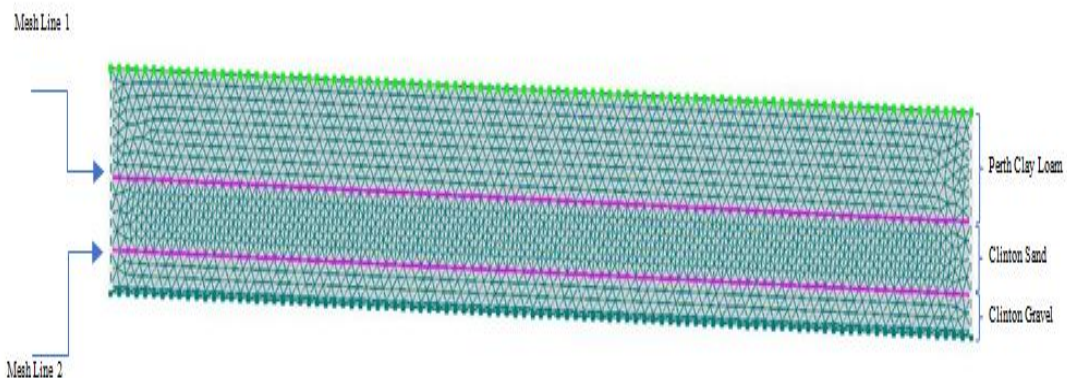


Fig. 2. Distribution of soil layers within the barrier (from top to bottom): Perth Clay Loam (60 cm); Clinton Sand (40 cm); Clinton Gravel (20 cm). An essential part of protective earthen cover is vegetation. In this present study evapotranspiration was indirectly

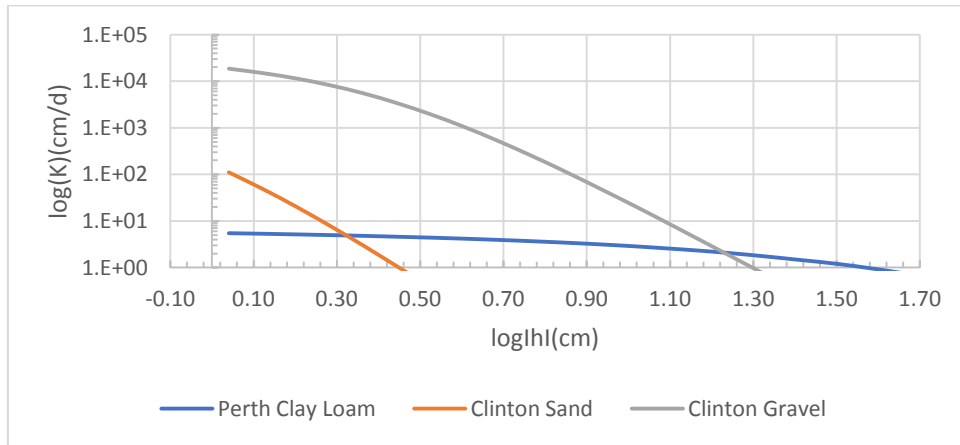


Fig. 4. Shows the soil water pressure head and hydraulic conductivity function obtained from equation (3) and (4)

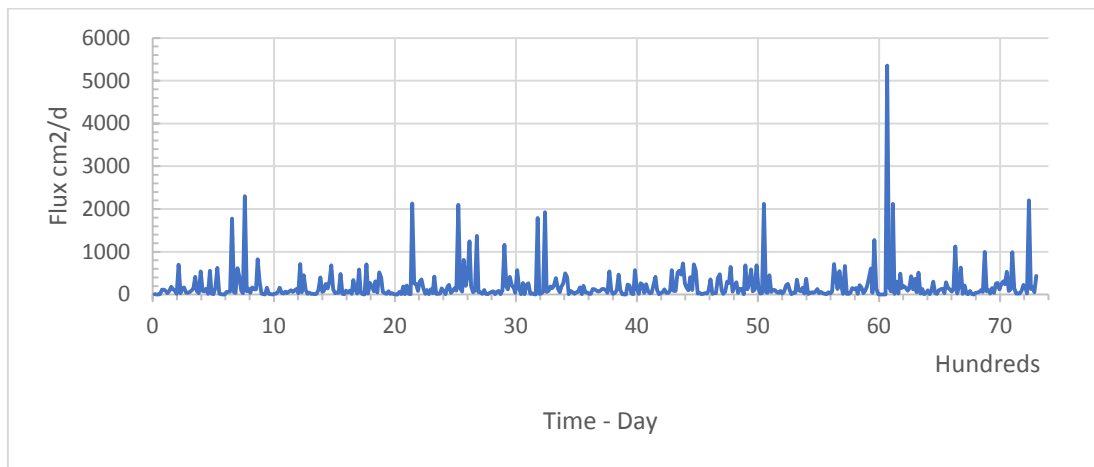


Fig. 5. Total flux across bottom boundary

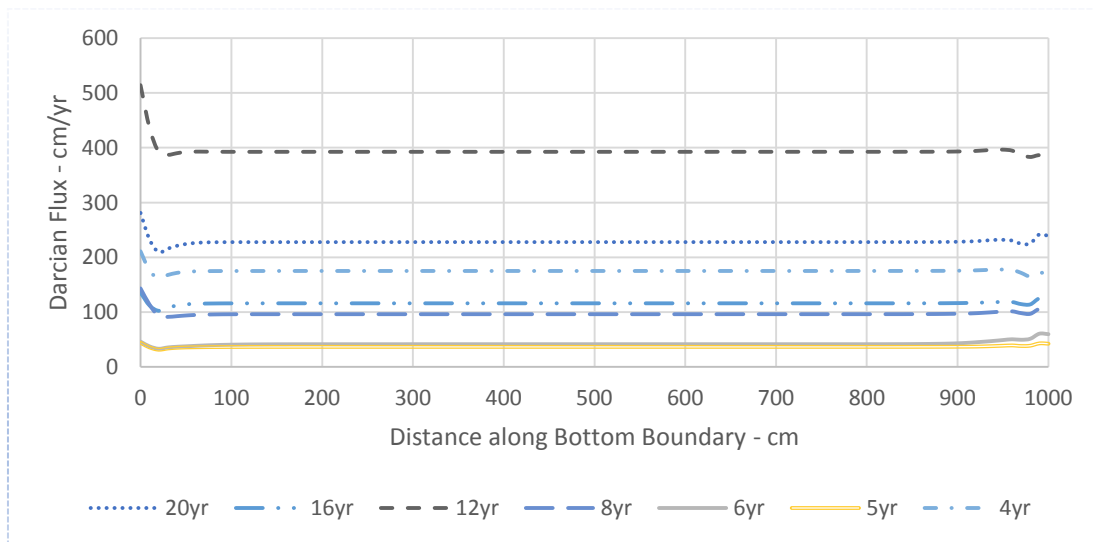


Fig. 6. Variation of the Darcian flux along the bottom boundary

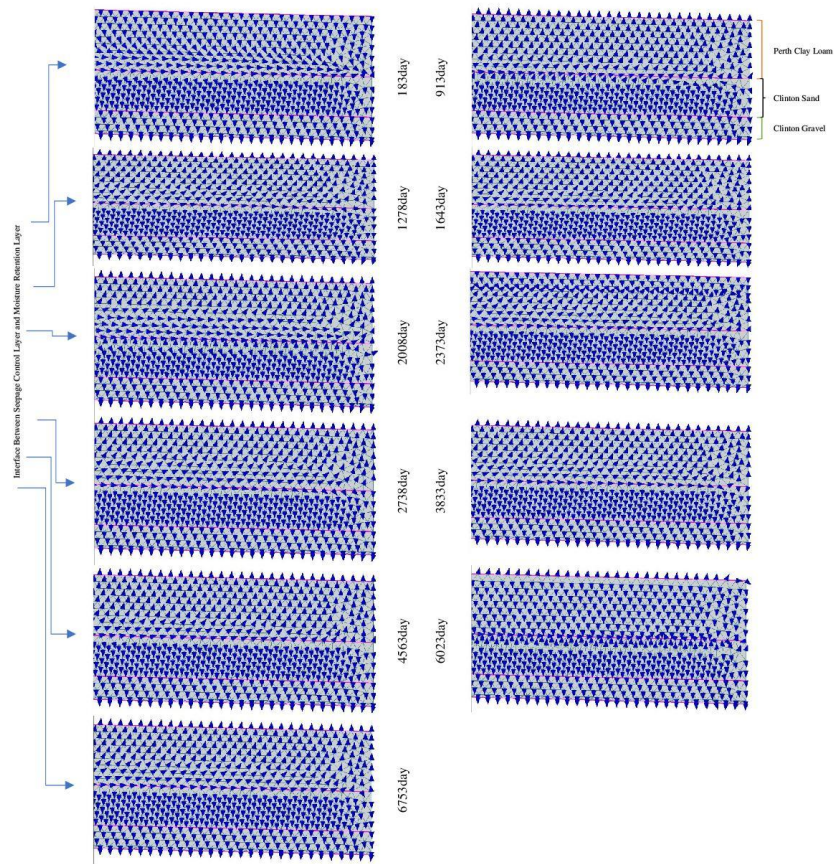


Fig. 7. Darcian velocity at eleven different times for various climatological conditions (Lateral drainage depicted in the interface between seepage control lyer and moisture retention layer)

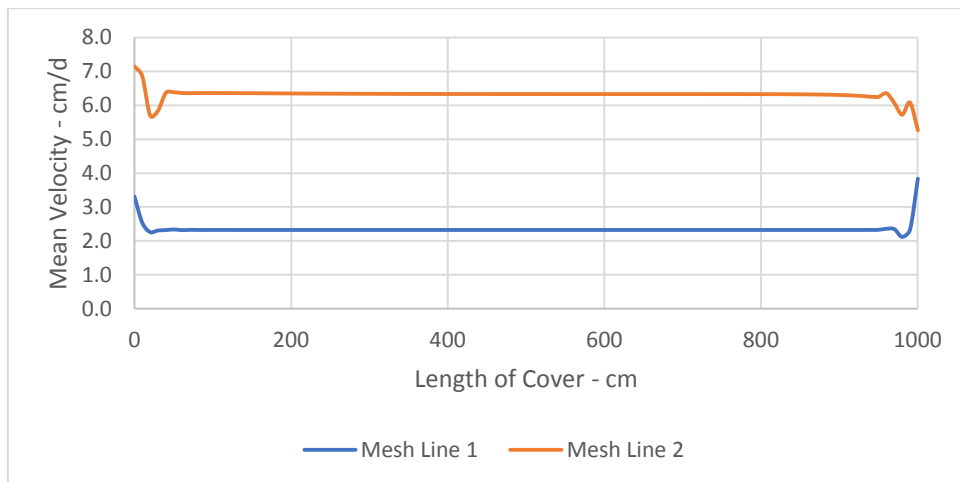


Fig 8. Flux Velocity across the bottom boundary at 867th week

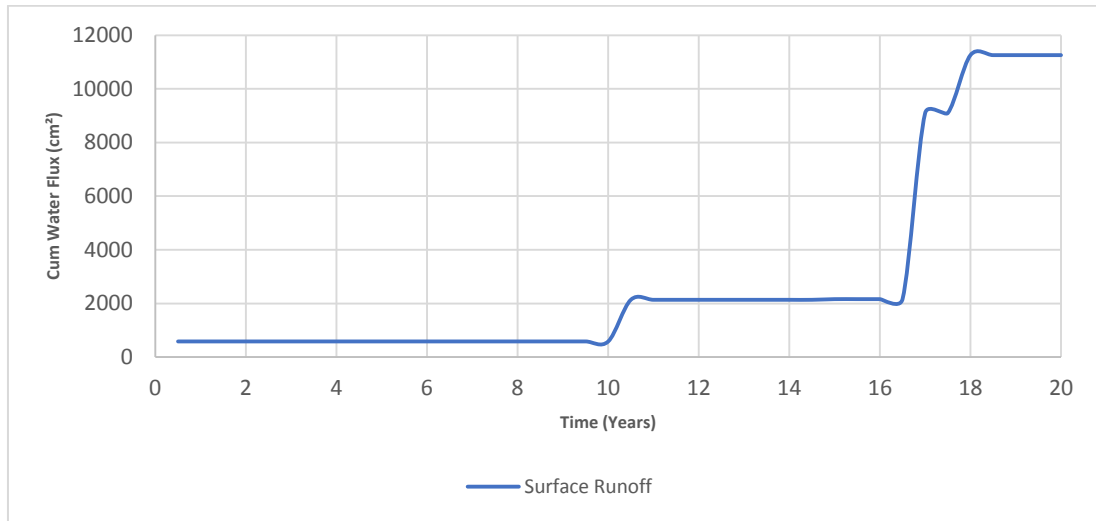


Fig. 9. Cumulative surface runoff

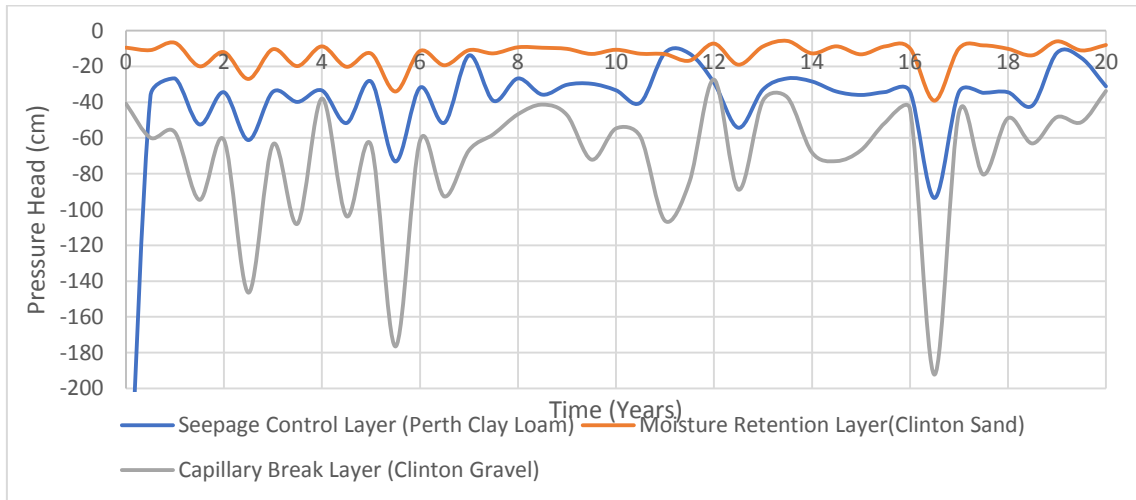


Fig. 10. Mean pressure head in layers

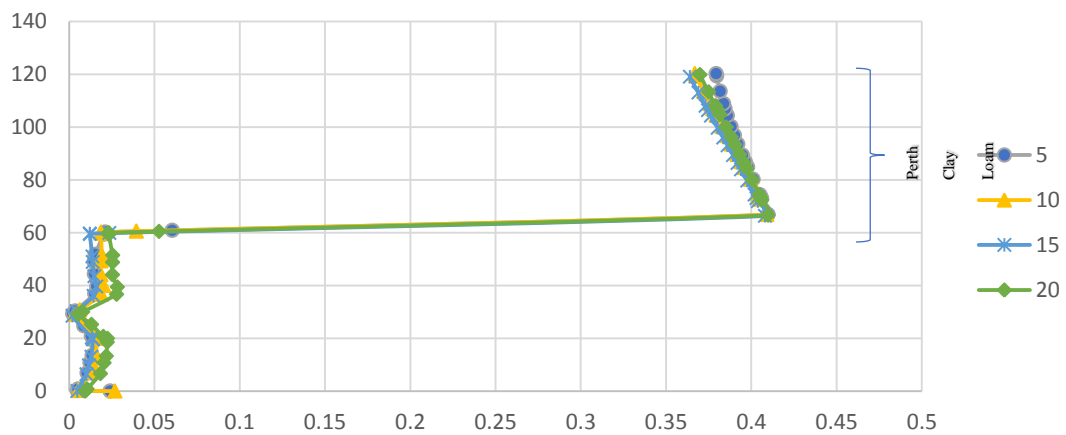


Fig. 11. Soil water content versus depth at four different times along a vertical line at x=250 cm from the left boundary

Table 1. Soil water retention and hydraulic conductivity parameters and initial soil water content (θ_i) for soil types used in the water flow calculations

Parameter	Perth Clay Loam	Clinton Sand	Clinton Gravel
Material number	1	2	3
Layer number	1	2	3
Layer thickness(cm)	60	40	20
$\theta_r(cm^3/cm^3)$	0.0696	0	0.0016
$\theta_s(cm^3/cm^3)$	0.4142	0.2323	0.2378
$\alpha (cm)^{-1}$	0.0115	1.1956	0.3580
n	1.4562	2.4925	2.1014
$K_s (\frac{cm}{d})$	7.37	3196.8	43200
Source	van Genuchten, M.Th., Leij, F.J., and Yates, S.R. [24], Richards and Morwick [9]	Parent 2003	Parent 2003
$\theta_i(cm^3/cm^3)$	0.2501	0.01138	0.01389
Source	Twarakavi, N. K. C, M. Sakai, and J. Šimůnek. 2009; Šimůnek, J., van Genuchten, M. Th. and Šejna, M. 2012		

Table 2. Summary of simulation results: hmean is mean pressure head,

		Layers		
		1	2	3
Time (day)	Property			
183	hMean	-36.35	-10.84	-59.80
913		-61.11	-27.03	-146.49
1278		-39.77	-19.81	-107.93
1643		-51.59	-20.19	-103.68
2008		-73.07	-34.07	-176.60
2373		-51.40	-19.37	-92.72
2738		-39.16	-12.67	-57.83
3833		-40.17	-12.89	-59.38
4563		-54.22	-19.00	-88.89
6023		-93.04	-39.18	-192.37
6753		-41.84	-13.79	-63.14

Conclusively, a lateral hydraulic gradient exists between the clay loam and sand, creating a lateral flux into the sand (Fig. 7). Based on the average flux across the bottom boundary (free drainage boundary condition) the highest mean velocity occurs in week 867 from 1043 weeks. Hence, the highest velocity in the respective time occurs at the bottom of the 3rd layer (it occurs 860 cm from the left boundary of the simulation). The lower peaks in the bottom layer are observed approximately 20 cm from the left boundary and 20 cm from the right boundary in the gravel layer (Fig.8).

Lastly, the cumulative flux across the bottom boundary was calculated. The total cumulative flux equals the summation of the fluxes of each element, times the element length (L^2T^{-1}). This was equal to $1505.5 cm^2/day$. This value equals

78.91% of the cumulative net rainfall that entered the barrier from the atmospheric boundary. Therefore, 21.09% of the rainfall can be considered runoff (Fig.9).

The simulated mean pressure head for all barrier layers at transient state was summarized in table 2.

As expected, the second layer (moisture retention layer) held more water, and the mean pressure head in the third layer held less, due to the high retention capacity of the sand layer and the lateral diversion phenomenon.

Based on Darcy fluid velocities (Fig.7), fluxes in the sand layer are parallel to the slope. In the intended times, the significant amount of water that passed through the sand layer was laterally

diverted. The capillary barrier effect was depicted at $t=2008$ days and $t=6023$ days when a considerable volume of water was diverted along the interface of the moisture retention layer and the capillary break layer. The capillary barrier effect was presented in the interface when the fine-grained material overlaid the coarse-grained one. In unsaturated conditions, the pressure head in the fine-grained layer was higher than the pressure head in the coarse-grained material. As a result, the moisture retention layer could store water. Furthermore, water was diverted laterally due to the slope of the layer. Based on the mean pressure head for various climatological conditions, the seepage control layer was -326.91 cm at its lowest and -11.75 cm at its highest (Fig.10). Based on the water retention curve shape of the clay loam (Fig.3), the negative pressure heads have a noticeable effect on water content and degree of saturation.

The profile of water content (Fig.11) along a perpendicular line at 250 cm from the left boundary of the earthen cover was depicted for changeable climatological conditions. In the first layer, the infiltration developed between $t=1825$ days and $t=7300$ days. The water content in the top 22.7 cm of the sand layer showed a steady-state behavior, but then reduced suddenly. This event is introduced as the main reason for the lateral diversion of water. The water content in the gravel layer was reduced as well, but its behavior was not linear, and the bottom of the layer was not saturated.

In this calculation, the distribution of hydraulic properties was assumed to be homogeneous.

4. CONCLUSIONS

Based on the numerical analysis results at transient state conditions, the lateral drainage of water occurred at the interface between the sand layer and the gravel layer. In the current transient state for variable climatological conditions, 21% of water infiltration was converted to lateral drainage. Also, the mean flux that permeated the bottom boundary was 206.70 cm/day ($2.39e-6$ m/s). Hence, this mean flux had minimal effect in the variable climatological conditions. The performance of this protective earthen cover can, then, be guaranteed due to the current climatological conditions.

The results of negative pressure head in the seepage control layer showed that this layer is usually under unsaturated conditions. Hence, this

circumstance will cause the formation of cracks in the clay.

Future studies should address the investigation of multi-layered earthen covers using experimental data from laboratory prototypes or field-scale studies. In such studies, numerical calculations – such as the ones presented here – may be appropriate in selecting improved barrier designs.

DATA AVAILABILITY STATEMENT

Some or all data, models, and code that support the findings of this study are available through the corresponding author upon reasonable request.

ACKNOWLEDGEMENTS

This research has been made possible entirely through personal funding.

COMPETING INTERESTS

Authors have declared that no competing interests exist.

REFERENCES

1. Khire M, Benson C, Bosscher P. Capillary Barriers: Design Variables and Water Balance. *Journal of Geotechnical and Geoenvironmental Engineering*. 2000; 126(8):695-708. DOI:10.1061/(ASCE)1090-0241(2000)126:8(695).
2. Ogorzalek A, Bohnhoff G, Shackelford C, Benson C, Apiwantragoon P. Comparison of Field Data and Water-Balance Predictions for a Capillary Barrier Cover. *Journal of Geotechnical and Geoenvironmental Engineering*. 2008; 134(4):470-486. DOI:10.1061/(ASCE)1090-0241(2008)134:4(470)
3. Ng C, Liu J, Chen R, Xu J. Physical and numerical modeling of an inclined three-layer (silt/gravelly sand/clay) capillary barrier cover system under extreme rainfall. *Waste Management*. 2015;38:210-221. DOI: 10.1016/j.wasman.2014.12.013
4. Zhan L, Qiu Q, Xu W, Chen Y. Field measurement of gas permeability of compacted loess used as an earthen final

- cover for a municipal solid waste landfill; 2016.DOI: 10.1631/jzus.a1600245
5. Chen R, Liu J, Ng C, Chen Z. Influence of Slope Angle on Water Flow in a Three-Layer Capillary Barrier Soil Cover under Heavy Rainfall. *Soil Science Society of America Journal*. 2019;83(6):1637-1647. DOI: 10.2136/sssaj2019.05.0135
 6. Chen R, Huang J, Leung A, Chen Z, Chen Z. Experimental Investigation on Water Release and Gas Emission of Evapotranspirative Capillary Barrier Landfill Covers. *Soil Science Society of America Journal*; 2021. DOI: 10.1002/saj2.20348
 7. Zaradny H. Groundwater flow in saturated and unsaturated soil. Edited by R.B. Zeidler. Balkema, Rotterdam, the Netherlands; 1993. Available:[https://www.cambridge.org/core/journals/journal-of-fluid-mechanics/article/groundwater...>](https://www.cambridge.org/core/journals/journal-of-fluid-mechanics/article/groundwater...)
 8. Morris CE, Stormont JC. Capillary barriers and Subtitle D covers: estimating equivalency. *Journal of Environmental Engineering*. 1997;123(1):3–10. DOI: 10.1061/(ASCE)0733-9372(1997)123:1(3)
 9. Bussière B, Aubertin M, Chapuis R. The behavior of inclined covers used as oxygen barriers. *Canadian Geotechnical Journal*. 2003;40(3):512-535. DOI: 10.1139/t03-001.
 10. Mallants D, Volckaert G, Marivoet J. Sensitivity of protective barrier performance to changes in rainfall rate. *Waste Management*. 1999;19(7-8):467-475. DOI: 10.1016/s0956-053x(99)00236-6
 11. Aubertin M, Cifuentes E, Apithy S, Bussière B, Molson J, Chapuis R. Analyses of water diversion along inclined covers with capillary barrier effects. *Canadian Geotechnical Journal*. 2009;46(10):1146-1164. DOI: 10.1139/t09-050
 12. Zaslavsky D, Sinai G. Surface Hydrology: III Causes of Lateral Flow. *Journal of the Hydraulics Division*. 1981a;107(1):37-52. DOI: 10.1061/jyceaj.0005605
 13. Zaslavsky D, Sinai G. Surface hydrology: IV — Flow in sloping, layered soil. *Journal of the Hydraulics Division, ASCE*. 2081b;107(HY1):53–64. DOI: 10.1061/jyceaj.0005606
 14. Nieber J, Walter M. Two-dimensional soil moisture flow in a sloping rectangular region: Experimental and numerical studies. *Water Resources Research*. 1981;17(6):1722-1730. DOI: 10.1029/wr017i006p01722
 15. Stagnitti F, Parlange J, Steenhuis T, Parlange M, Rose C. A mathematical model of hillslope and watershed discharge. *Water Resources Research*. 1992;28(8):2111-2122. DOI: 10.1029/92wr00705
 16. Selim H. Water Flow in Layered Soils with Sloping Surface. *Journal of Irrigation and Drainage Engineering*. 1988;114(3):442-462. DOI:10.1061/(asce)0733-9437(1988)114:3(442)
 17. Steenhuis T, Parlange J, Sanford W, Heilig A, Stagnitti F, Walter M. Can we distinguish Richards' and Boussinesq's equations for hillslopes?: The Coweeta Experiment revisited. *Water Resources Research*. 1999;35(2):589-593. DOI: 10.1029/1998wr900067
 18. Tang J, Taro U, Huang D, Xie J, Tao S. Physical Model Experiments on Water Infiltration and Failure Modes in Multi-Layered Slopes under Heavy Rainfall. *Applied Sciences*. 2020;10(10): 3458. DOI: 10.3390/app10103458
 19. Li N, Jiang H, Li X. Behaviour of Capillary Barrier Covers Subjected to Rainfall with Different Patterns. *Water*. 2020;12(11): 3133. DOI: 10.3390/w12113133
 20. Todd D. *Groundwater Hydrology*; JonWiley & Sons Inc.: New York, NY, USA, 1980;103. Available:[https://www.scirp.org/%28S%28i43dyn45teexjx455qIt3d2q%29%29/referen ce/referencespapers.aspx?referenceid=2518382>](https://www.scirp.org/%28S%28i43dyn45teexjx455qIt3d2q%29%29/referen ce/referencespapers.aspx?referenceid=2518382)
 21. McCord JT, Stephens DB, Wilson JL. Toward validating state-dependent macroscopic anisotropy in unsaturated media: Field experiments and modeling considerations, *J. Cont. Hydrol*. 1991; 7:145– 175. DOI: 10.1016/0169-7722(91)90042-Y
 22. Assouline S, Nicpon M, Huber D. The Impact of Vulnerabilities and Strengths on the Academic Experiences of Twice-Exceptional Students: A Message to School Counselors. *Professional School Counseling*. 2006;10(1):14-24. DOI: 10.5330/prsc.10.1.y0677616t5j15511
 23. Yeh H, Tsai Y. Analyzing the Effect of Soil Hydraulic Conductivity Anisotropy on Slope

- Stability Using a Coupled Hydromechanical Framework. *Water*. 2018;10(7):905. DOI: 10.3390/w10070905
24. Šimůnek J, van Genuchten M. Th, Šejna M. The HYDRUS Software Package for Simulating the Two- and Three-Dimensional Movement of Water, Heat, and Multiple Solutes in Variably Saturated Porous Media (Technical Manual Version 2.0); 2012. Available at: < <https://www.pc-progress.com/en/default.aspx?hydrus-3d>>
25. Jensen D, Hargreaves G, Temesgen B, Allen R. Computation of ETo under Nonideal Conditions. *Journal of Irrigation and Drainage Engineering*. 1997;123(5):394-400. DOI: 10.1061/(asce)0733-9437(1997)123:5(394)
26. Šimůnek J. Estimating groundwater recharge using HYDRUS-1D. In: *Engineering geology and Hydrogeology*, Sofia. 2015;25–36. Available: https://www.pc-progress.com/Documents/Jirka/Simunek_EnginGeolHydrogeol_2016.pdf>
27. Ritchie J. Model for predicting evaporation from a row crop with incomplete cover. *Water Resources Research*. 1972;8(5):1204-1213. DOI: 10.1029/wr008i005p01204
28. Asaadi A, Arora V, Melton J, Bartlett P. An improved parameterization of leaf area index (LAI) seasonality in the Canadian Land Surface Scheme (CLASS) and Canadian Terrestrial Ecosystem Model (CTEM) modelling framework. *Biogeosciences*. 2018;15(22):6885-6907. DOI: 10.5194/bg-15-6885-2018.
29. van Genuchten M, Leij FJ, Yates SR. The RETC Code for Quantifying the Hydraulic Functions of Unsaturated Soils. Vol. EPA/600/2-. U.S. Department of Agriculture, Agriculture Research Service; 1991. Available at: < <https://www.epa.gov/water-research/retention-curve-retc-computer-program>>
30. Van Genuchten M. A Closed-form Equation for Predicting the Hydraulic Conductivity of Unsaturated Soils. *Soil Science Society of America Journal*. 1980;44(5):892-898. DOI: 10.2136/sssaj1980.0361599500440005002x
31. Mualem Y. A new model for predicting the hydraulic conductivity of unsaturated porous media. *Water Resources Research*. 1976;12(3):513-522. DOI: 10.1029/wr012i003p00513
32. Neuman SP, Feddes RA, Bresler E. Finite Element Simulation of Flow in Saturated-Unsaturated Soils Considering Water Uptake by Plants. 3rd Annual Report, Project No. A10-SWC-77, Hydraulic Engineering Laboratory Technicon, Haifa; 1974.
33. Twarakavi NKC, Sakai M, Šimůnek J. An objective analysis of the dynamic nature of field capacity, *Water Resources Research*. 2009;45,W10410:9. DOI: 10.1029/2009WR007944

© 2021 Hagh Shenaa and Sharafi; This is an Open Access article distributed under the terms of the Creative Commons Attribution License (<http://creativecommons.org/licenses/by/4.0>), which permits unrestricted use, distribution, and reproduction in any medium, provided the original work is properly cited.

Peer-review history:
The peer review history for this paper can be accessed here:
<https://www.sdiarticle5.com/review-history/81417>